Correlation of Radiation Creep Theory with Experimental Evidence

W.G. Wolfer

May 1979

UWFDM-312

J. Nucl. Matls. 90, 175-192 (1980).

Correlation of Radiation Creep Theory with Experimental Evidence

W.G. Wolfer

Fusion Technology Institute
University of Wisconsin
1500 Engineering Drive
Madison, WI 53706

http://fti.neep.wisc.edu

May 1979

UWFDM-312

J. Nucl. Matls. 90, 175-192 (1980).

Correlation of Radiation Creep Theory
with Experimental Evidence

by

W. G. Wolfer

UWFDM-312

Invited paper presented at the International Conference on Fundamental Mechanisms of Radiation-Induced Creep and Growth, Chalk River, Canada, May 1979.

Abstract

A review is presented of theoretical models related to irradiation creep and to the evolution of the dislocation structure in irradiated stainless steels. The results of detailed analysis for stress-induced loop alignment and stress-induced preferential absorption (SIPA) of point defects at dislocations is presented.

Stress-induced rotation of tri-interstitials is shown to be too small to account for the observed variations in loop densities on different crystallographic planes. However, it is possible to predict large variations with the SIPA mechanism.

Predictions of irradiation creep by the SIPA mechanism are in agreement with measured data at intermediate fluences. At low fluences, additional contributions to irradiation creep must come from dislocation glide. The evolution of the dislocation structure can be explained by the continuous formation of interstitial type loops and by the radiation-induced recovery of the dislocation network.

1. Introduction

1.1 The Need for Theoretical Correlations

A critical comparison between predictions of theoretical models of irradiation creep with experimental observations and data is essential for a better understanding of the physical basis of irradiation creep. That it is also necessary for the proper utilization of experimental results to the design of reactors is perhaps not obvious. Therefore, we mention some of the critical issues one faces when experimental data of irradiation creep are analyzed and applied to reactor design.

Perhaps the most obvious example demonstrating the need for a mechanistic understanding is the problem of formulating a general irradiation creep law for a triaxial stress state. Irradiation creep data are obtained in experiments with easily realizable stress states, such as in pressurized tubes, uniaxial tension, or in helical springs or leaf springs. The information obtained for these specific stress states must all be condensed into one constitutive law applicable to any state of stress, in accordance with theoretical principles.

This task is complicated by radiation-induced dimensional changes which may be superimposed on the creep strains. The theoretical analysis must be employed to aid in the separation of strains due to three distinct phenomena which may occur simultaneously; these are stress-affected swelling, anisotropic growth, and irradiation creep.

Theory is further called upon to formulate creep laws for complicated stress and temperature histories. Most irradiation creep experiments are conducted with constant loads and temperature. In rare cases, tests with simple load or temperature histories have been conducted. The most burning questions in this context are related to the nature of the transient creep strains. A mechanistic understanding of the irradiation creep process is needed to separate the permanent plastic deformation from anelastic strains which are recoverable after load removal.

Another critical issue is the superposition of irradiation creep, thermal creep, and plastic flow. All three deformation models are encountered under abnormal operation conditions which must be analyzed in order to insure the safety of nuclear reactors. The rules of superposition strongly affect the safety analysis. Since in-reactor experiments can simulate accident conditions only to a limited degree, our theoretical understanding must provide the superposition rules.

An important problem that theory must address is related to the difference between post-irradiation and in-reactor creep rupture and fatigue failure. Recent experiments [1] clearly demonstrated the beneficial effect that irradiation creep has in improving the stress-rupture time. Since grain boundary cavity formation is a prerequisite of creep rupture, an understanding of the interplay between irradiation creep and grain boundary sliding and cavitation may provide the key to predict in-reactor fracture.

These are but a few of the outstanding problems which demand a better theoretical understanding of irradiation creep. Answers to these problems posed above still await further research. Nevertheless, the critical comparison presented in this paper between the theoretical predictions and the experimental data may already provide important insights.

1.2 Stratification of the Theory

Various mechanisms for irradiation creep have been proposed in the past with various degrees of sophistication. A review of the models reveals that their components can be divided into four categories depending on a dimensional scale. Each scale defines a level of inquiry, and we refer to them as the atomistic, the microstructural, the micromechanical, and the macromechanical level. On each level, different mechanistic models are involved, and they contribute to the macroscopic irradiation creep behavior of a material. Table 1 gives a list of those models. In order to derive theoretically the constitutive law for irradiation creep, the modeling must be started at the atomistic level and, in an ascending progression, be carried through all following levels.

It is important to realize this stratification of the mechanistic approach to irradiation creep and growth, as there are observable creep effects which do not, for example, involve any processes on the atomistic level. We shall discuss an example in Section 4.

Starting at the atomistic level, the basic processes capable of causing permanent lattice deformation are the stress-induced alignment of small dislocation loops or interstitial clusters, the stress-induced growth of dislocation loops, the unfaulting process of Frank loops, the climb of edge dislocations, and finally the glide of dislocations.

The electron microscopy observations of the dislocation structure in irradiated and stressed metals do not reveal directly the atomistic process behind irradiation creep. It must be inferred from the microstructural record. However, even if this is not possible, electron microscopy observations can give us quantitative information about the sink structure, their number density, and its evolution as a function of dose and temperature. This information is invaluable when quantitative predictions are required to test the viability of

Table 1. Stratification of the Mechanistic Inquiry about Irradiation Creep

Level of Inquiry	Mechanistic Models
Atomistic Processes	Alignment of Dislocation Loops Formation and Growth of Loops Dislocation Climb Unfaulting of Frank Loops Dislocation Glide
Microstructural Processes	Intersection and Coalescence of Loops Loop-Dislocation Interaction Precipitates on Loops and Dislocations Dislocation Network Formation and Recovery
Micro-mechanics	Dependence on Crystal Orientation Grain to Grain Interaction Grain Boundary Sliding Grain Boundary Cavity Formation Roberts-Cottrell Creep
Macro-mechanics	Averaging over Many Grains Phenomenological Considerations

a certain atomistic process for irradiation creep. In particular, the temperature and dose dependence of irradiation creep will be seen to be determined primarily by the corresponding dependence of the loop and dislocation densities.

To understand the evolution of the dislocation structure, a variety of processes must be considered. These include the intersection of loops, either with other loops or with network dislocations, the glide resistance imposed by sessile Frank loops on dislocations, the interaction of loops and dislocations with precipitate particles and voids, and the change of the dislocation density by radiation-induced recovery.

A comprehensive experimental study of the microstructural evolution has only recently become available in the pioneering work of Brager et al. [2,3,4]. Their work contains sufficient details about microstructural parameters to guide the theoretical development and to allow a meaningful comparison of theoretical predictions and the observed irradiation creep behavior. In the following,we shall heavily rely on their work.

Based on the atomistic and microstructural processes, it can be concluded that the irradiation creep rate depends on the crystal orientation with respect to the applied loads. This has recently been shown by Wolfer and Garner [5] in the case of ion-bombarded surfaces. They have demonstrated that the state of stress in the bombarded layer depends on the orientation of the surface grain. In the case of a neutron irradiated polycrystalline material the grain to grain variation of irradiation creep may result in residual microstresses. Depending on their magnitude, they may affect the formation and growth of grain boundary cavities and cracks. Furthermore, these microstresses must be taken into consideration when one interprets the microstructural records in stressed specimens.

Internal stresses are also generated if anisotropic irradiation growth occurs which varies from location to location. Residual stresses generated by such a process have recently been suggested as a cause for irradiation creep [6]. This particular mechanism is based on ideas put forth by Roberts and Cottrell [7] for irradiation creep in α-uranium. This particular creep mechanism requires no detailed description of the atomistic process involved except for the assumption that it is glide. However, for a clear demonstration of the viability of this mechanism it is necessary that a detailed micromechanical analysis is carried out for a polycrystal. Unfortunately, such an analysis is still lacking. The irradiation creep models based on the idea of internal stresses employ mostly intuitive and suggestive arguments rather than rigorous ones.

The Robert-Cottrell mechanism is a case in point that the macroscopic creep law must be derived by an appropriate averaging of the creep behavior of many grains joined together in a compatible way. When this is done, a macroscopic creep law emerges with new terms not present at the micromechanical level. These terms describe the anelastic effects caused by the residual microstresses, and they have the appearance of a transient creep effect when load changes occur. However, they are distinct from transient creep strains which contribute permanently to the deformation. The interpretation of transient strains requires therefore that the anelastic effects be subtracted.

In the following sections we shall elaborate only on those models listed in Table 1 for which some definite and lasting progress has been made, and for which some experimental evidence can be cited to support it.

2. Atomistic Processes for Irradiation Creep

2.1 Stress-Induced Loop Alignment

It was proposed by several investigators [8,9,10,11] that a stress-induced alignment of dislocation loops would cause irradiation creep. However, with the exception of the vacancy cluster collapse models [8,9], no specific atomistic processes were given that would lead to this alignment. Instead, it was simply conjectured that in the presence of a stress field σ_{ij}, the number of loops on a crystallographic plane with normal vector $\hat{n}$ ($\hat{n}^2 = 1$) would be proportional to a Boltzmann factor

$$N_\ell(\hat{n}) = N_\ell^o \exp\left(\pi R_o^2 b\, \sigma_n/kT\right), \qquad (1)$$

where

$$\sigma_n = \sum_{ij} \hat{n}_i \hat{n}_j \sigma_{ij} \qquad (2)$$

is the normal stress on the loop plane, b is the Burger's vector, and R_o is the critical radius of the loop. Two opposite assumptions can be made with regard to N_ℓ^o; it can either be the number of loops in the stress-free crystal or it can be normalized such that the total loop density on all planes remains independent of stress. In the former case, the total interstitial loop density is enhanced by a tensile stress, whereas in the latter case, the same number of loops is merely partitioned unequally on the various crystallographic planes.

The implications of the latter model to irradiation creep have been analyzed by Brailsford and Bullough [11] who pointed out that the deformation produced by aligned loops is equivalent to anisotropic growth without stress. The stress would only be required initially. However, it was suggested by

Wolfer and Boltax [12] that the state of anisotropy would only persist for the lifetime of interstitial loops. As they continuously form, grow, unfault, and merge with the dislocation network, any preferred loop orientation would eventually be replaced by a new one dictated by the present state of stress. The transitory existence of interstitial loops appears to be confirmed now by the experimental evidence of the evolution of the dislocation structure [4] with dose. Therefore, stress-induced loop alignment and lack of a stress memory in irradiation creep is no longer contradictory. Nevertheless, there remains the open question whether the dislocation network resulting from an aligned loop structure preserves part of the anisotropy in the form of a preferred Burgers vector orientation.

The first experimental observation of different loop densities on different $\{111\}$ planes in a stressed sample of SA 316 stainless steel [13] was initially thought to confirm a loop alignment mechanism. However, as has been shown recently [14], and as will be elaborated upon further in this paper, these observations are also in agreement with the mechanism of stress-induced preferential absorption (SIPA).

In these early observations, made on a sample from a pressurized tube irradiated at 380°C to a rather low fluence of $2.4 \times 10^{25} n/m^2$, it was found that the loop radius at the maximum of the size distribution was nearly independent of the normal stress σ_n. However, the height of the size distribution did depend on the stress, and it was enhanced by up to 32% on some planes and suppressed as much as 28% on other planes in comparison to the average height.

In searching for a physical process for loop alignment we have considered two possibilities: the stress-assisted rotation of interstitial clusters, and the stress-induced change of the loop nucleation rate. Garner et al. [15] have recently explored the latter possibility by adapting the void nucleation theories of Katz, Wiedersich and Russell to interstitial loop nucleation. They showed that there exists no nucleation barrier (i.e. a positive maximum value of the free energy defined in a kinetic theory) beyond the di-interstitial cluster. Furthermore, since the binding energy of a di-interstitial in nickel is 1.16 eV according to calculations by Johnson [16], the probability for its dissociation is small. Therefore, the corresponding nucleation barrier at the di-interstitital stage is small. Finally, as will be shown below, stress changes the bias factor of loops of all sizes, and is then more appropriate to describe the effect of stress in terms of loop growth.

It appears then that there remains only the possibility for loop alignment by stress-induced reorientation of small interstitial clusters. Evidence for such a stress-assisted rotation in Al has been found recently by Robrock et al. [17] using internal friction and elastic-aftereffect techniques. They concluded that reorientation of the di-interstitial is associated with migration. Five other observed relaxation peaks were shown to be due to the rotation of one or more members of a cluster, but not associated with long-range migration of this cluster. In particular, one of the more pronounced peaks was tentatively assigned to the reorientation of the middle interstitial in a tri-interstitial cluster configuration. This reorientation produces two identical configurations of tri-interstitial as shown in Fig. 1. By the addition of more interstitials these configurations can presumably evolve into dislocation loops with different orientations.

The activation energy for reorientation is of the order of 0.1 eV. This is sufficiently low so that we can assume an equilibrium distribution of the number of tri-interstitials with a given orientation. This number is proportional to

$$A = \exp\,[P_{ij}^{(3)}\,\tilde{\varepsilon}_{ij}/kT] \qquad (3)$$

where $P_{ij}^{(3)}$ is the dipole tensor of a tri-interstitial and $\tilde{\varepsilon}_{ij}$ is the deviatoric elastic strain tensor.

The proposed configuration of the tri-interstitial is shown in Fig. 1 in its six possible orientations. The middle interstitial can rotate, whereupon each of three configurations on the left-hand-side of Fig. 1 is converted into those of the right-hand-side and vice versa. We assume now that the dipole tensor $P_{ij}^{(3)}$ for each configuration can be obtained as a superposition of the dipole tensor $P_{ij}^{(2)}$ of the di-interstitial and the dipole tensor $P_{ij}^{(1)}$ of the single interstitial.

Robrock et al. [17] have determined the anisotropies of these dipole tensors and found the following values for Al: for the di-interstitial,

$$|P_{11}^{(2)} - P_{22}^{(2)}| \geq 6 \text{ eV},$$

and for the single interstitial

$$|P_{11}^{(1)} - P_{22}^{(1)}| \cong 1.1 \pm 0.3 \text{ eV} .$$

Although we cannot determine the dipole tensor $P_{ij}^{(3)}$ with these values, we can evaluate the deviatoric dipole tensor

$$\tilde{P}_{ij}^{(3)} = P_{ij}^{(3)} - \frac{1}{3}\,\delta_{ij}P_{kk}^{(3)} ,$$

in the following manner.

For the tri-interstitial in the upper left-hand corner of Fig. 1, we find with the above assumption that

$$P_{11}^{(3)} = P_{22}^{(1)} + P_{22}^{(2)} \ , \quad P_{22}^{(3)} = P_{11}^{(1)} + P_{22}^{(2)} \ , \quad P_{33}^{(3)} = P_{11}^{(1)} + P_{22}^{(2)}$$

if the (11)-components are parallel to the dumbbell axis. Then

$$\tilde{P}_{11}^{(3)} = -\frac{1}{3}\{P_{11}^{(1)} - P_{22}^{(1)} + P_{11}^{(2)} - P_{22}^{(2)}\} \cong -2.4 \text{ eV} ,$$

$$\tilde{P}_{22}^{(3)} = \frac{1}{3}\{2P_{11}^{(1)} - 2P_{22}^{(1)} - P_{11}^{(2)} + P_{22}^{(2)}\} \cong -1.3 \text{ eV} ,$$

$$\tilde{P}_{33}^{(3)} = \frac{1}{3}\{-P_{11}^{(1)} + P_{22}^{(1)} + 2P_{11}^{(2)} - 2P_{22}^{(2)}\} \cong 3.6 \text{ eV} .$$

By permutation of these three values, the deviatoric components of the dipole tensors can be obtained for the other five configurations. We assume that the above values reflect the order of magnitude for tri-interstitials in all fcc metals, including austenitic stainless steels. The alignment factor A of Eq. (3) for the biaxial stress state in a pressurized tube is given by

$$A = \exp \{\frac{\sigma_\theta}{4GkT} (-\tilde{P}_{11}^{(3)} + \tilde{P}_{22}^{(3)})\} \ , \qquad (4)$$

where σ_θ is the hoop stress and G the shear modulus. When Eq. (4) is evaluated for a hoop stress of about 200 MPa and a temperature of 380°C, the pertinent conditions for the experiment in Ref. [13], we obtain the values listed in the last column of Table 2.

Although the tri-interstitials cannot be identified directly with an embryonic loop, they must represent precursors, and their stress-induced alignment should reflect the degree of alignment of interstitial loops. We see from Table 2 that at the most an 8% alignment can be assigned to tri-interstitials, whereas a 30% alignment was found for the

Table 2

Tri-interstitial Dipole Tensors and Alignment Factors

Configuration in Fig. 2	Components of Dipole Tensor (eV) $\tilde{P}_{11}^{(3)}$	$\tilde{P}_{22}^{(3)}$	$\tilde{P}_{33}^{(3)}$	Alignment Factor
a	-2.4	-1.3	3.6	1.015
a'	-2.4	3.6	-1.3	1.083
b	-1.3	-2.4	3.6	0.985
b'	3.6	-2.4	-1.3	0.923
c	-1.3	3.6	-2.4	1.068
c'	3.6	-1.3	-2.4	0.937

interstitial loops in Ref. [13]. To explain the larger alignment it would be necessary to require a fourfold increase in the anisotropy of the dipole tensor for a tri-interstitial or an impurity-interstitial complex which may also serve as a precursor to an interstitial loop. Although this is not outside the realm of plausibility, it would be difficult to explain much larger degrees of alignment of loops as seen at higher fluences.

High fluence observations were made by Brager et al. [4] on pressurized tubes of type 316 stainless steels both in the annealed and the cold-worked condition, and they can be explained, as shown below, in terms of stress-induced loop growth.

2.2 The Stress-Induced Preferential Absorption

2.2.1 The Dislocation Bias Factors

The stress-induced preferential absorption (SIPA) of interstitials at dislocations (and to a lesser degree of vacancies) has been proposed independently by Heald and Speight (HS) [18] and Wolfer and Ashkin (WA) [19,20]. Bullough and Willis (BW) [21] have also analyzed the stress-induced interaction energy of point defects with edge dislocations and proposed an approximate form for it which was used by Heald and Speight [22] to determine the stress-induced bias factor and SIPA creep. Although the point of departure is the same, the treatments of WA and HS differ not only in their approach but also in their final results by almost an order of magnitude. Therefore, some clarifying statements are in order.

The origin of the SIPA mechanism is the modulus interaction of a point defect with an edge dislocation. Since this interaction energy is quadratic in the total strain field, there appears a cross-term in it when a uniform strain field due to external loads is superimposed on the strain field of the dislocation. This cross-term is linear in both strain fields, and given by [20]

$$\delta E(r,\phi) = \frac{b}{r}\,[A_1\cos\phi + A_3\cos3\phi + B_1\sin\phi + B_3\sin3\phi] \ , \qquad (5)$$

where b is the Burgers vector, and (r,ϕ) are the polar coordinates of the point defect in a cylindrical coordinate system with the edge dislocation located along the axis.

The constants in this expression are

$$A_1 = A_3 = \alpha^G\,\tilde{\varepsilon}_{xy}/[2\pi(1-\nu)] \qquad (6)$$

$$B_3 = \alpha^G\,(\tilde{\varepsilon}_{yy} - \tilde{\varepsilon}_{xx})/[4\pi(1-\nu)] \qquad (7)$$

$$\begin{aligned} B_1 &= -\alpha^K\,\varepsilon_{kk}(1-2\nu)/[2\pi(1-\nu)] \\ &\quad -\alpha^G\,[\tilde{\varepsilon}_{xx}(3-4\nu) + \tilde{\varepsilon}_{yy}(1-4\nu)]/[4\pi(1-\nu)], \end{aligned} \qquad (8)$$

where

$$\tilde{\varepsilon}_{ij} = \varepsilon_{ij} - \frac{1}{3}\,\delta_{ij}\,\varepsilon_{kk} \qquad (9)$$

is the deviatoric elastic strain tensor due to the external loads, $\varepsilon_{kk} = \varepsilon_{11} + \varepsilon_{22} + \varepsilon_{33}$ is the corresponding elastic dilatation, ν is the Poisson's ratio, and α^K and α^G are the bulk and shear polarizability, respectively, of the point defect.

In the treatments of HS and BW, only special cases of Eq. (5) are considered, namely for a uniaxial external stress parallel and perpendicular to the Burgers vector of an edge dislocation; the terms with A_1 and A_3 are thereby suppressed.

The gradient of δE contributes to the drift term of the diffusion equation. This equation must be solved with the entire interaction energy included. For the case of a straight edge dislocation, the diffusion problem can be solved in closed form only if the entire interaction energy has the spacial dependence $\sin\phi/r$. Apparently motivated by the desire to also cast δE is this form, BW approximatesterms with angular functions $\sin^3\phi$ and $\sin\phi \cos^2\phi$ by terms with $\frac{1}{2} \sin\phi$. This approximation of δE can then simply be included into the size-interaction. In so doing, HS obtain then a bias factor Z which can be expressed in terms of zero order Bessel functions, the argument of which is given by $c/2a$. c is a capture radius which depends on the entire interaction energy, and a is a cut-off radius of the order of the dislocation core radius. HS now make the further assumption that $c >> a$, and they proceed to approximate the modified Bessel function by a logarithmic function. Unfortunately, as has been shown earlier [20], this latter approximation is incorrect as c is of the same order as a.

In the perturbation treatment of WA none of these dubious approximations have been made, and the bias factor obtained is valid for any triaxial strain field, and hence, also for any orientation of the dislocation.

The perturbation treatment to third order gives the following result for the bias factor of a straight edge dislocation:

$$Z^d(\sigma) = Z^d(o) + \delta Z^d(\sigma_H) = \delta Z^d(\tilde{\sigma}) \quad . \tag{10}$$

The first term is the bias factor in the absence of an external load, whereas

$$\delta Z^d(\sigma_H) = - \frac{(b/4a)^2}{\ell n(d/a)} \left[\frac{1-2\nu}{2\pi(1-\nu)kT}\right]^2 \alpha^{k}v\sigma_H \tag{11}$$

and*

$$\delta Z^d(\tilde{\sigma}) = - \frac{1}{3} \frac{(b/4a)^2}{\ell n(d/a)} \frac{(1+\nu)\ \alpha^{G}v}{[2\pi(1-\nu)kT]^2} [2\hat{b}_i\hat{b}_j - (1-4\nu)\hat{\ell}_i\hat{\ell}_j]\ \tilde{\sigma}_{ij} \tag{12}$$

---

*Repeated indices imply a summation as usual.

are stress-induced contributions to the bias due to the hydrostatic stress

$$\sigma_H = \frac{1}{3} (\sigma_{11} + \sigma_{22} + \sigma_{33}) \qquad (13)$$

and due to the deviatoric stress

$$\tilde{\sigma}_{ij} = \sigma_{ij} - \delta_{ij}\sigma_H \quad , \qquad (14)$$

respectively.

In Eqs. (11) and (12), 2d represents the mean distance between dislocations, v the relaxation volume of the point defect, kT is the thermal energy, and $\hat{b}_i$ and $\hat{\ell}_i$ are the components of unit vectors parallel to the Burgers vector and to the dislocation line, respectively.

The stress-induced contribution $\delta Z^d(\sigma_H)$ is independent of the orientation of the dislocation or its Burgers vector, and will have no effect on irradiation creep, but only on swelling. On the other hand, the contribution $\delta Z^d(\tilde{\sigma})$ does not affect swelling, but it gives rise to creep. Henceforth, we shall only deal with this term.

In case of an infinitesimal dislocation loop, the perturbation treatment has to be carried out only to second order to obtain the stress-induced contribution. The bias factor for the faulted loop is given by

$$Z^\ell(\sigma) = Z^\ell(o) + \delta Z^\ell(\tilde{\sigma}) \quad , \qquad (15)$$

where the stress-induced part is

$$\delta Z^\ell(\tilde{\sigma}) = - \frac{3\alpha^G/G}{128(1-\nu)kT} \frac{b}{R} \hat{b}_i \hat{b}_j \tilde{\sigma}_{ij} \quad . \qquad (16)$$

Here, G is the shear modulus and R the loop radius.

In closing this section it is noted that the above expressions are valid for elastically isotropic materials and for point defects with isotropic dipole and polarization tensors.

2.2.2 The SIPA Creep Rate

The rate of deformation (including swelling) produced by the climb of edge components for both Frank loops and line dislocations is given by

$$\begin{aligned}\dot{\varepsilon}_{ij} &= \Omega \int d\omega_b \, N^{\ell}(\hat{b}) \, (J_I^{\ell} - J_V^{\ell}) \, \hat{b}_i \hat{b}_j \\ &+ \Omega \int d\omega_{\ell} \int d\omega_b \, N^{d}(\hat{\ell},\hat{b}) \, (J_I^{d} - J_V^{d}) \, \delta(\hat{b}\cdot\hat{\ell}) \, \hat{b}_i \hat{b}_j \ ,\end{aligned} \tag{17}$$

where Ω is the atomic volume, and $(J_I - J_V)$ is the difference in the interstitial and vacancy currents.

The integrations are carried out over the solid angle ω_b of the Burgers vector orientations, and in the case of edge dislocations, also over the solid angle ω_{ℓ} of the line vector orientation subject to the condition that $\hat{b}$ is perpendicular to $\hat{\ell}$.

If either of the two densities, $N^{\ell}(\hat{b})$ for the loops, or $N^{d}(\hat{\ell},\hat{b})$ for the dislocations, depends on the crystallographic orientation, $\dot{\varepsilon}_{ij}$ will not be isotropic even in the case of no external stress. In this case, swelling would be anisotropic. Furthermore, irradiation creep would also be anisotropic, and would not obey the Lévy-von Mises relationships; i.e., $\dot{\varepsilon}_{ij}$ would not be proportional to $\tilde{\sigma}_{ij}$.

Since the Burgers vector has discrete crystal orientations, Eq. (17) will not yield an isotropic creep law even if loop densities and dislocation densities have no preferred Burgers vectors. For a polycrystalline cubic material with no texture, we must include into the integration of Eq. (17) also the integration over all possible grain orientations. We may accomplish this by simply allowing Burgers vectors of any orientation. With no preferred Burgers vector orientations, N^{ℓ} and N^{d} are constants, and the integration can be carried out easily.

The expressions $(J_I^\ell - J_V^\ell)$ and $(J_I^d - J_V^d)$ for the net flow of atoms to Frank loops or dislocations can be derived from the general formula valid for any sink, namely

$$J_I^s - J_V^s = A^s Z_V^s \{[\frac{Z_I^s}{Z_V^s} - \frac{\bar{Z}_I}{\bar{Z}_V}] F + D_V(C_V^s - \overline{C_V^s})\} \quad . \tag{18}$$

Here

$$F = (\bar{N}\ \bar{Z}_V/2K)\{(L^2 + M)^{1/2} - L\} \tag{19}$$

$$L = 1 + K\ D_V\overline{C_V^s}/\bar{N}\ \bar{Z}_I \tag{20}$$

$$M = 4K\ P/\bar{N}^2\bar{Z}_I\bar{Z}_V \quad . \tag{21}$$

Furthermore, the recombination coefficient is given by

$$K = 4\pi r_c/D_V \tag{22}$$

where r_c is the capture radius of a vacancy for interstitials. The additional parameters are listed and defined in Table 3 and 4. Sink-averaged quantities, indicated by a bar, are defined in the following manner. The total sink density is

$$\bar{N} = \sum_s N^s A^s \tag{23}$$

where the geometric factors A^s are given in Table 4. Average bias factors are defined as

$$\bar{Z} = \sum_s N^s A^s Z^s\ /\bar{N}\ , \tag{24}$$

and the average thermal vacancy concentration as

$$\overline{C_V^s} = \sum_s N^s A^s Z_V^s C_V^s/(\bar{N}\bar{Z}_V) \tag{25}$$

With the help of Table 4, the net flow of atoms can be determined according to Eq. (18), and inserted in Eq. (17). In performing the

Table 3. Parameters for Ni or γ-Fe

Parameter	Symbol	Value or Definition
Vacancy formation energy	E_V^f	1.6 eV
Vacancy migration energy	E_V^m	1.4 eV
Burgers vector (γ-Fe)	b	2.50×10^{-10} m
Atomic volume	Ω	b^3
Equilibrium vacancy concentration	C_V^{eq}	$(1/\Omega)\exp(1.5-E_V^f/kT)$ m^{-3}
Vacancy diffusion coefficient	D_V	$1.53\times10^{-4}\exp(-E_V^m/kT)m^2s^{-1}$
Shear modulus	G	10^{11} J/m^3
Poisson's ratio	ν	0.3
Relaxation volumes	v	$v_I/\Omega=1.4$, $v_V/\Omega=-0.2$
Shear polarizabilities	α^G	α_I^G = -150 eV, α_V^G = -15 eV
Recombination radius	r_c	4b
Core cut-off radius	a	7b (for interst.), 4b (for vac.)
Defect production rate	P	$= 7.5*10^{-22}$ ϕ η [dpa/s]
Fast neutron flux	ϕ	$\approx 2\times10^{15}[cm^{-2}s^{-1}]$ for EBR-II
Cascade survival fraction	η	0.6

Table 4. Definitions for Loops and Dislocations and Their Contributions to the Deformation Rate

Quantity	for Frank Interstitial Loop	for Edge Dislocation
Geometric factor	$A^\ell = 8\pi R$, R is the loop radius	$A^d = 2\pi/\ell n\,(d/a)$ 2d is the dislocation spacing
Sink density	N^ℓ [number per unit volume]	N^d [number per unit area]
Bias factor	Equations (15) and (16)	Equations (10), (11), and (12)
Thermal vacancy concentration	$C_V^\ell = C_V^{eq} \exp \{\frac{\Omega}{kT} [\hat{b}_i \hat{b}_j \sigma_{ij} - \frac{dW/dR}{2\pi Rb}]\}$ Loop energy $W = \frac{G\ b^2}{18(1-\nu)} R[\ell n \frac{4R}{b} + 2\ell n 2 - 1] + \pi R^2 \gamma_{SF}$ γ_{SF} is the stacking fault energy	$C_V^d = C_V^{eq} \exp \{\frac{\Omega}{kT} \hat{b}_i \hat{b}_j \sigma_{ij}\}$ $\hat{b}_i \hat{b}_j \sigma_{ij} = \sum_{ij} \hat{b}_i \hat{b}_j \sigma_{ij}$
Net flow of atoms	Equation (18), $(J_I^\ell - J_V^\ell)$ is the net flow per loop	Equation (18), $(J_I^d - J_V^d)$ is the net flow per unit length
Angular averaged thermal vacancy concentration	$\bar{C}_V^\ell = C_V^{eq} \exp \{\frac{\Omega}{kT} (\sigma_H - \frac{dW/dR}{2\pi Rb})\}$ $\sigma_H = \frac{1}{3} (\sigma_{11} + \sigma_{22} + \sigma_{33})$	$\bar{C}_V^d = C_V^{eq} \exp \{\Omega \sigma_H / kT\}$
Swelling contribution, $\frac{\dot{S}}{3} \delta_{ij}$	$\Omega N^\ell\ 8\pi R\ Z_V^\ell(o)\ \{\Delta Z^\ell\ F + D_V\ (\bar{C}_V^\ell - \bar{C}_V^s)\}$	$\frac{\Omega \pi N^d}{3\ell n(d/a)} Z_V^d(o)\ \{\Delta Z^d\ F + D_V\ (\bar{C}_V^d - \bar{C}_V^s)\}$
Net bias	$\Delta Z_o^\ell = Z_I^\ell(o)/Z_V^\ell(o) - \bar{Z}_I/\bar{Z}_V$	$\Delta Z_o^d = Z_I^d(\sigma_H)/Z_V^d(\sigma_H) - \bar{Z}_I/\bar{Z}_V$
SIPA contribution, $\dot{\varepsilon}^{IC}$	$N^\ell\ \tilde{\sigma}_{ij}\ \xi^\ell\ \{\Delta Z_s^\ell\ F - \alpha_V^G\ D_V(\bar{C}_V - \bar{C}_V^s)\}$	$N^d\ \tilde{\sigma}_{ij}\ \xi^d\ \{\Delta Z_s^d\ F - \alpha_V^G \upsilon_V D_V(\bar{C}_V^d - \bar{C}_V^s)\}$
Stress-induced net bias	$\Delta Z_s^\ell = -\ \alpha_I^G + \alpha_V^G\ \bar{Z}_I/\bar{Z}_V$	$\Delta Z_s^d = -\alpha_I^G \upsilon_I + \alpha_V^G \upsilon_V\ \bar{Z}_I/\bar{Z}_V$
Proportionality factor	$\xi^\ell = \frac{\Omega \pi b}{80(1-\nu)kT}$	$\xi^d = \frac{\Omega \pi}{90} \frac{(1+\nu)(5-4\ )}{[2\pi(1-\nu)kT]^2} [\frac{b/4a}{\ell n(d/a)}]^2$
Thermal creep contribution, $\dot{\varepsilon}^{TC}$	$\frac{8\pi}{15} N^\ell R \frac{\Omega^2 \tilde{\sigma}_{ij}}{kT} Z_V^\ell(o)\ D_V \bar{C}_V^\ell$	$\frac{A^d}{30} N^d \frac{\Omega^2 \tilde{\sigma}_{ij}}{kT} Z_V^d(\sigma_H)\ D_V \bar{C}_V^d$

angular integrations we retain only terms linear in the deviatoric stress tensor. The total strain rate is then found to be a sum of three terms

$$\dot{\varepsilon}_{ij} = \frac{1}{3}\delta_{ij}\dot{S} + \dot{\varepsilon}^{IC}_{ij} + \dot{\varepsilon}^{TC}_{ij} , \qquad (26)$$

i.e., a sum of swelling, irradiation creep, and thermal creep of the Nabarro type. Frank loops and dislocations each make separate contributions to all three processes, and their corresponding expressions are listed in Table 4.

The creep rate $\dot{\varepsilon}^{IC} + \dot{\varepsilon}^{TC}$ can be computed from known microstructural data. Using the data for SA 316 by Brager and Straalsund [2], predictions for the creep rate were made earlier by Wolfer [23]. Based on the experimental information known at that time, the conclusion was reached that SIPA irradiation creep could not account for the measured creep rates below a fast neutron fluence of 2 x 10^{26} n/m^2. In the meantime, however, new experimental results frompressurized tubes have revealed that the irradiation creep rate does indeed increase with fluence. Hence, these earlier predictions [23] based on SIPA and the observed microstructure appear now to be substantiated after all, at least in principle. We shall, therefore, reexamine the issue.

To facilitate the comparison, the accumulated creep strain, or rather $\varepsilon/(\sigma/G)$, is shown in Fig. 2 as computed with the SIPA model and the fluence- and temperature-dependent microstructural data [2]. Experimentally measured data for SA 316 pressurized tubes [24] are also shown in Fig. 2. The predictions follow the trend of the data rather well. However, the measured creep strains at T = 425°C are substantially higher than the predicted ones, particularly at low fluences. Contrarily, at T = 475°C, the computed creep strains are somewhat higher than the measured ones for fluences above 2 x 10^{26} n/m^2.

Several points must be noted here. First, the microstructural data used were from small rod samples not under stress. Any effect of stress on the microstructure is therefore missing. Second, the material for the rod samples and for the pressurized tubes were from different heats. Considering the large heat to heat variations of measured irradiation creep strains [25], the difference between the predicted and measured creep strains is not at all surprising.

The accelerating irradiation creep rate predicted by the SIPA mechanism is attributed to the rapid increase of the dislocation density in solution-annealed materials. Based on this interpretation, one would expect that the irradiation creep rate in the cold-worked material should be substantially larger than in the annealed material and decelerate with increasing fluence. The reason for this expected difference is that the dislocation density in 20% cold-worked 316 SS decreases rapidly and reaches a saturation level within a fluence interval of about 1×10^{26} n/m^2. We shall discuss shortly this radiation-induced recovery of the dislocation density.

It is evident from Fig. 2 that no decelerating creep rate is observed in 20% CW 316 SS. Although its initial creep rate is somewhat larger initially, it seems to follow essentially the same trend as the creep rate of the annealed material. One may explain this similarity of the creep rate in two ways. First, the dislocations in the cold-worked material are incapable of climbing under irradiation, because they may be effectively pinned by impurity atoms or small precipitate particles. However, this would contradict the observed recovery of the dislocation density.

A second explanation can be derived from the heterogeneous distribution of the cold-worked structure. The individual dislocations are members of dense tangles, and were formed during the cold-working by the same Frank-Read sources. Their Burgers vectors are therefore parallel or antiparallel to each other. Their bias is then equally affected by the external stress. Lacking a nearby partner with different Burgers vectors and hence different stress-induced bias, no SIPA couples exist. Hence, the planar multipole configurations of edge dislocations seen in cold-worked materials are not capable of participating in the SIPA creep.

The temperature dependence of the SIPA creep is derived to a large extent from the temperature dependence of the dislocation and loop densities, and to a lesser extent from the temperature dependence of the point defect concentrations and the stress-induced bias factors. Since the dislocation densities in both annealed and cold-worked materials are of comparable magnitude at high fluences and temperatures, the temperature dependence is also expected to be similar. This is shown in Fig. 3. The SIPA predictions are again based on the microstructural data [2] for solution-annealed type 316 stainless steel, whereas the actual creep rate data [24] are from pressurized tubes of 20% CW 316. The agreement is rather satisfactory at temperatures above 450°C. Below this temperature, the discrepancy between the predictions and the data may again be due to the differences in heat treatment.

At very high temperatures, the irradiation creep rate is overtaken by the thermal creep rate according to the Nabarro mechanism. Since the dislocation density under irradiation is higher than in the unirradiated annealed material, Nabarro-creep is in fact enhanced under irradiation.

In summary, the SIPA mechanism can account for a substantial fraction, if not for all, of irradiation creep at fluences greater than 10^{26} n/m^2 in type 316 stainless steels. There appears to be some deficiency at lower fluences, where glide processes may be contributing significantly to irradiation creep. It is important to note that among the parameters that enter the theoretical SIPA predictions, the shear polarizability α_I^G of an interstitial is the least known. Although measured values exist of the magnitude used here, they are for the stable configuration of the interstitial rather than the saddle-point configuration. Furthermore, these values are not for stainless steels. It appears then that the ultimate success of the SIPA mechanism as an explanation for irradiation creep depends on a better knowledge of this critical parameter.

2.3 Irradiation Creep Mechanisms Based on Glide

If dislocations climb because of the preferred absorption of either interstitials or vacancies they will inevitably glide to some extent. This will even happen in the absence of external loads, and the glide motion is directed entirely by the internal stress fields. These internal stress fields are generated by the dislocations themselves and their arrangement, and they are responsible for the long-range interaction among dislocations. They are also contributing to the yield strength of the material, and they may be considered as a source for glide obstruction.

Medium and short-ranged glide obstacles are created by sessile dislocation loops, by small defect clusters, and by precipitate particles. If the density of these glide obstacles is sufficiently high to fill the spaces between the glide dislocations, they will dominate the glide resistance.

Irradiation creep models based on glide may be categorized according to the nature of the glide obstacles and their range of interaction with the dislocations, and according to the cause of the climb that releases the dislocation from the obstacle. Table 5 presents a list of the glide models for irradiation creep together with their stress dependence.

Table 5

Glide Models for Irradiation Creep

Cause of Climb Glide Obstacle	Radiation-Induced	Stress-Induced
Short-Ranged	Climb-controlled glide (CCG) σ, σ^{n-1}	SIPA-controlled glide (PA) σ^2
Medium-Ranged	Climb around Frank loops (CCG) $\sigma^{1/2}$, σ	Unlikely
Long-Ranged	Climb-induced yield (CIY) σ	Most Unlikely

For the case of short-ranged glide obstacles and radiation-induced climb, it is tempting to simply modify the corresponding thermal creep models for alloys. The third power stress dependence for thermal creep reduces then to a σ^2-law for irradiation creep. More generally, the thermal creep power n would be diminished by one for irradiation creep.

All these third power models for thermal creep must utilize the fact that either the mobile dislocation density is proportional to σ^2 or that the subgrain size diminishes with stress. Thermal creep models with stress-powers $n > 3$ are based on dislocation pile-ups and planar multipoles which are continously fed by Frank-Read sources.

In order to obtain a linear stress dependence for irradiation creep by climb-controlled glide (CCG) Gittus [26] makes the ad hoc assumption that the area swept out in the glide process, after the dislocation is released from the obstacle, is simply proportional to the elastic bow-out, i.e., to the applied stress. This implies that the planar obstacle density on the glide plane decreases with the applied stress.

Mansur [27] coupled the CCG model of Gittus with the SIPA process and deduced a quadratic stress dependence. The SIPA-controlled glide in his model obviates the need for a net preferential absorption of interstitials at all edge dislocations. Hence, irradiation creep proceeds also in the absence of swelling.

If it is assumed that the glide dislocation density as well as the average obstacle distance are independent of stress, a CCG-model with short-ranged obstacles would give the absurd result that irradiation creep is independent of stress above the value of the Peierls friction stress. This demonstrates in a dramatic way that it is important to consider the force distance relationship between the obstacle and the glide dislocation. For any given applied load, there exists a sphere of influence around the obstacle at the boundary of which the obstacle force equals the line tension of the dislocation. Since the obstacle force becomes stronger closer to the obstacle, the number of effective obstacles intersecting the glide plane as well as their effective height decreases with increasing stress. Wolfer and Boltax [12] have applied these considerations to the case where small Frank loops constitute the major glide obstacles. They derived two stress dependencies: $\sigma^{1/2}$ and σ. The former would be expected only for very small stresses when dislocation pile-ups are unlikely to occur, whereas the linear stress dependence requires the formation of pile-ups.

They also pointed out that an increasing loop density with increasing radiation dose will reduce the CCG contribution to irradiation creep. Consequently, CCG is expected to be active only at low doses.

Since the effective height of the obstacle which must be overcome by climb is rather large in the case of Frank loops, it is unlikely that SIPA could proceed at a sufficient rate to release the glide dislocations. Therefore, we expect that obstacles with medium-ranged interaction forces can be overcome only by swelling-driven climb or by random climb based on differences in the intrinsic bias factor of dislocations in different environments [28].

The long-range forces between dislocations have recently been implicated [6] as the cause of irradiation creep. Adopting the idea for the Robert-Cottrell creep to cubic metals, Gittus [6] has argued that a climbing network can be considered as a source of internal stresses whose distribution is nonuniform and continuously fluctuating. The dislocations are subject to the stochastic internal stress field and perform a random glide motion which can be biased in one direction by an externally applied load. In spite of the model's intuitive appeal, however, there remain some serious questions as to its validity. The major objection that can be raised is that forces between any two dislocations are equal and opposite. If σ_i is the internal stress generated by all other climbing dislocations, the total stress acting on one given dislocation is $(\sigma-\sigma_i)$ where σ is the external stress. If the specific glide contribution of any given dislocation is proportional to $(\sigma-\sigma_i)$, the average glide contribution is proportional to $(\sigma-\bar{\sigma}_i)$. The average internal stress, $\bar{\sigma}_i$, is zero because of balance of forces. Hence, dislocation interactions can have no effect on the irradiation creep rate. This conclusion was in fact reached by Weertman [29] in conjunction with thermal creep.

In concluding this short review on the role of glide, it is noted that climb-controlled glide of dislocations past obstacles is indeed an important mechanism for irradiation creep. However, theoretical models proposed so far are heuristic in nature, and depending on the assumptions, yield a variety of stress dependencies.

3. Microstructural Processes

3.1 The Evolution of the Dislocation Network

The formation and growth of interstitial-type loops is one of the most conspicuous manifestations of radiation damage in metals at elevated temperatures. Because dislocation loops have a bias factor for interstitial absorption greater than the bias factor for straight edge dislocations, interstitial loops continue to grow until they coalesce or react with the network dislocations. Exceptions to this unlimited growth may occur when impurities segregate to the loops, and at high temperatures, when thermal vacancies diffuse to the interstitial loops.

In a well annealed material the maximum radius R_m to which the loops can grow is determined by $(4\pi/3)\ N^{\ell}\ R_m^3 \cong 1$, where N^{ℓ} is the loop density. Coalescence and unfaulting of the loops produces a network of dislocations. As the dislocation density increases, the loops react more and more with the network than with each other. One would expect then that the maximum loop radius is of the order of the mesh length $\rho^{-1/2}$, where ρ is the dislocation density. Such a relationship has indeed been observed [4] for neutron irradiated type 316 stainless steels.

The continued production of dislocations by the growing interstitial loops is eventually balanced by the radiation-induced recovery of the network dislocation density. To describe then the evolution of the dislocation density N^d, models for the impingement rate of loops on the network must be developed and models for the radiation-induced climb must be used to compute the annihilation of edge dislocations with opposite Burgers vector.

Instead of presenting a detailed theoretical account we adopt here a simple phenomenological approach. First, in analogy to thermal recovery, it is assumed that the recovery rate under irradiation is also proportional to $(N^d)^2$. The production rate of new dislocations, depending on the reaction between the growing loops and the network dislocations, is assumed to be proportional to N^d. Hence, we obtain as the rate equation for the dislocation density the relation

$$\frac{d}{dt} N^d = BN^d - A(N^d)^2 \quad . \qquad (27)$$

The function A is proportional to the climb rate of edge dislocations, whereas the function B is proportional to the growth rate of interstitial loops.

Both functions depend, apart from minor but essential differences in bias factors, on the net atom flux $(D_I C_I - D_V C_V)$. Their ratio, B/A, is then to a first approximation independent of the irradiation temperature for $T \leq 0.5\ T_m$. Above a temperature of $0.5\ T_m$, thermal recovery becomes important and B/A should decrease with increasing temperature. As a consequence of this model, the saturation value of the dislocation density

$$N_s^d = B/A \tag{28}$$

is expected to be independent of the irradiation temperature as long as the thermal recovery is negligible compared to the radiation-induced recovery.

If N_0^d is the initial dislocation density the solution of Eq. (27) is given by

$$N^d(t) = N_s^d/[1+(N_s^d/N_0^d-1)\exp(1-AN_s^d t)] \quad . \tag{29}$$

This equation describes the experimental observations of Brager et al. [30] rather successfully. The experimental results are shown in Fig. 4 for both solution annealed and cold-worked type 316 stainless steel neutron irradiated at T ≃ 500°C; the curves represent merely hand-drawn lines. The observed saturation dislocation density is $N_s^d = 6 \times 10^{10}\ \mathrm{cm}^{-2}$.

Using this value for the ratio B/A and the requirement that the dislocation density in the solution-annealed material reaches the saturation value N_s^d at a fluence of about $3 \times 10^{26}\ (\mathrm{n/m}^2)$, Eq. (29) gives the results as shown in Fig. 5. The initial dislocation densities were $N_0^d = 4 \times 10^8\ \mathrm{cm}^{-2}$ and $N_0^d = 7 \times 10^{11}\ \mathrm{cm}^{-2}$ for the solution-annealed and the cold-worked material, respectively. It is remarkable that this simple model, when fitted to two experimental values for the solution-annealed materials, predicts successfully the reduction of the dislocation density in the cold-worked material.

It contradicts, on the other hand, the notion that the original dislocations in the cold-worked material are in any way different from those produced during the irradiation, with regard to their ability to absorb point defects. Any differences between the irradiation creep rates of solution-annealed and cold-worked materials must then be attributed to the arrangement of groups of dislocations (multipoles vs. isolated dislocations) and/or the differences in the solute atom distribution in the matrix. The latter is known to be influenced by cold-working.

3.2 The Loop Size Distributions

It was shown earlier [14] that the number of loops formed by x interstitials, g(x,t), satisfies a Fokker-Planck equation

$$\frac{\partial g}{\partial t} = - \frac{\partial}{\partial x} \{\mathcal{F}(x) - \frac{\partial}{\partial x} \mathcal{D}(x)\} \; g(x,t) \qquad (30)$$

where

$$\mathcal{F}(x) = A^{\ell}(x) Z_V^{\ell}(x) [(Z_I^{\ell}/Z_V^{\ell} - \bar{Z}_I/\bar{Z}_V)F - D_V(\overline{C_V^s} - C_V^{\ell})] \qquad (31)$$

$$\mathcal{D}(x) = \frac{1}{2} A^{\ell}(x) Z_V^{\ell}(x) [(Z_I^{\ell}/Z_V^{\ell} + \bar{Z}_I/\bar{Z}_V)F + D_V(\overline{C_V^s} + C_V^{\ell})] \qquad (32)$$

The equation (30) can be solved by integrations when $\partial g/\partial t = 0$, as described in Ref. [14]. At temperatures below 500°C the terms containing the equilibrium vacancy concentrations C_V^{ℓ} and $\overline{C_V^s}$ may be neglected. Then, $\mathcal{F}/\mathcal{D}$, which determines to a large extent the shape of the loop size distribution, is then only dependent on the bias factor ratio $Z_I^\ell(x)/Z_V^\ell(x)$ and the average bias factor ratio $\bar{Z}_I/\bar{Z}_V$.

Previous computations [19] of the bias factors Z_I^ℓ and Z_V^ℓ were based on the infinitesimal loop approximation for the stress fields. The obtained results are therefore applicable only to small loops. In another investigation [20], corresponding bias factors were obtained for the straight edge dislocation. These two results can be considered to represent limiting cases of the bias factors for a finite circular dislocation loop. Unfortuately, only numerical results are available in this case [31]. In order to obtain a simple analytical expression, the following interpolation procedure was developed.

In the absence of any interaction of the point defect with the stress field of the loop, the point defect current can be written in the form

$$J = \frac{4\pi^2 R}{\ell n(8R/a)} D\ (C - C^s) \qquad (33)$$

where a is the core cut-off radius and R the loop radius. Seeger and Goesele [32] have shown that Eq. (33) is an excellent approximation to an exact result expressed in terms of toroidal harmonics. The geometry factor

$$A^\ell = 4\pi^2 R/\ell n(8R/a) \qquad (34)$$

bears great resemblance to the one for a straight edge dislocation, A^d, as listed in Table 4. In fact, if A^ℓ is divided by the circumference $2\pi R$, the geometry factor per unit length is $2\pi/\ell n(8R/a)$.

The dislocation bias could now be included into the expression for A^ℓ if the core cut-off radius were replaced by the capture radius C_I or C_V. Alternatively, we define a loop bias factor separately by

$$Z^{\ell}_{I,V} = \ell n(8R/a)/\ell n(8R/c_{I,V}) \quad , \qquad (35)$$

and determine the capture radii c_I and c_V and the core cut-off radius a such that Eq. (35) agrees with the previously derived bias factors for the infinitesimal loop as (R/b) becomes small, and with the bias factors for the edge dislocation as 2R approaches the average separation distance 2d of dislocations. The results so obtained are shown in Fig. 6. The solid lines are bias factors for the stress-free case, whereas the dashed lines show bias factors for a tensile stress of $\sigma/G = 10^{-3}$ normal to the loop plane. A tensile stress enhances the bias factor for interstitials slightly more than for vacancies. Compressive stresses result in a corresponding reduction of Z^{ℓ}_{I} and, to a lesser degree, of Z^{ℓ}_{V}.

In addition to the bias factors, we need the following boundary conditions for a solution of the steady-state equation $\partial g/\partial t = 0$. At a maximum loop radius of $R_m \cong 40$ nm, corresponding to a maximum interstitial number of $x_m = \pi(R/b)^2 \cong 10^5$, the loops are assumed to impinge on the network dislocation. This value of the maximum radius R_m was chosen in accord with the experimental observations of Brager et al.[4] shown in Figs. 7 and 8. The number of loops with this radius $g(x_m)$, becomes equal to zero.

At the lower end of the loop size distribution the loop density must become equal to the number of interstitial clusters $g(x_0)$ which constitute the embryonic loops. Since g(x) is proportional to $g(x_0)$, the normalized size distribution $g(x)/g(x_0)$ becomes equal to one as x approaches x_0. The following results are therefore presented in terms of the ratio $g(x)/g(x_0)$.

The last parameter needed to compute the loop size distribution is the ratio of the sink-averaged bias factors $\bar{Z}_I$ and $\bar{Z}_V$. Since the loops themselves contribute to these average bias factors, it would be necessary to not only know the loop size distribution first, but also the density and individual bias factors of all the other sinks present. Such a self-consistent evaluation of $\bar{Z}_I$ and $\bar{Z}_V$ is only possible in a comprehensive microstructural theory, which has not yet been developed.

For the sake of demonstrating the effect of stress on the loop size distributions, we consider the ratio $\bar{Z}_I/\bar{Z}_V$ as an input parameter. Its value must be larger than the bias factor ratio Z_I^d/Z_V^d for edge dislocations when loops are present, and it is therefore equal to $Z_I^\ell(x^*)/Z_V^\ell(x^*)$, where x^* is the number of interstitials in the average loop size. We select this average loop size to coincide with the maximum of the experimental loop size distribution of Fig. 7, i.e., at a radius of about $R^* = 32.5$ nm. This corresponds to a value $x^* \cong 13300$.

With all the above specifications the loop size distribution can now be computed as discussed previously [14], and the results are shown in Fig. 9. The three normalized size distributions $g(x)/g(x_0)$ are for the stress-free case (o), and a normal tensile (+) or compressive (-) stress of $\sigma_n = \pm 10^{-3}G$, respectively.

In comparing these theoretical results with those in Fig. 8, it must be noted that the loop bias factor contribution leading to SIPA and to the stress-induced change of the loop size distribution is dependent upon the normal deviatoric stress

$$\sigma_{dn} = \sum_{ij} \tilde{\sigma}_{ij} n_i n_j = \sigma_n - \sigma_H$$

where σ_H is the hydrostatic stress.

In a pressurized tube, the deviatoric normal stress on planes perpendicular to the radial direction is equal to $(-\sigma_\theta/2)$, where σ_θ is the hoop stress. The deviatoric normal stress on planes perpendicular to the axial direction is equal to zero, and on planes perpendicular to the hoop direction $\sigma_{dn} = + \sigma_{\theta}/2$.

Based on the theoretical predictions, the loop size distribution in pressurized tubes should then be below and above the "stress-free" size distribution. The experimental observations shown in Fig. 8 agree in principle with this conclusion, although the suppression on planes nearly perpendicular to the radial direction is less than the enhancement on planes oriented nearly perpendicular to the hoop direction. This asymmetry in the "splitting" of the loop size distributions in pressurized tubes is associated with an overall increase in the total number of loops present compared to the number in stress-free tubes.

Stress-induced rotation of the embryonic loop density $g(x_o)$ could produce an asymmetric splitting but it would not result in an enhancement of the overall loop density. One would therefore be led to the conclusion that tensile normal stresses should also enhance the number $g(x_o)$ of embryonic loops. Although both the asymmetry and the increase in loop density could thereby be explained, the above theoretical analysis requires further refinements before a firm conclusion can be reached. First, there exists of course a range of radii at which the loops become part of the dislocation network rather than one unique value R_m. Second, the unfaulted loops as well as the network dislocations may glide under the influence of the stress, and thereby affect the range of maximum loop radii. Third, we have neglected entirely the interaction and the possible reaction of loops on different crystallographic planes. In spite of all these omissions, the present theoretical explanation of the loop size distributions in stressed materials is considered to be one of the strongest supports for the existence of the SIPA mechanism for irradiation creep.

4. Micro- and Macromechanics

As indicated in section 2, the constitutive equation for creep within one grain depends on the orientation of the climb or glide systems with regard to the stress state. This crystallographic dependence arises from two reasons. First, there exist only a discrete number of glide systems and climb directions in a cubic crystal. Therefore, as shown recently [5], the creep strain rate tensor $\dot{\varepsilon}_{ij}$ is related to the deviatoric stress tensor $\tilde{\sigma}_{k\ell}$ by a creep compliance tensor $\psi_{ijk\ell}$ such that

$$\dot{\varepsilon}_{ij} = \sum_{k\ell} \psi_{ijk\ell} \, \tilde{\sigma}_{k\ell} \quad . \tag{36}$$

In materials with microstructures having no preferred Burgers vectors, the creep compliance tensor shares the symmetry properties of the crystal lattice, rendering the creep properties anisotropic.

An additional anisotropy is produced in $\psi_{ijk\ell}$ if the dislocation structure exhibits a preferred Burgers vector. An example is provided by the splitting of the loop size distributions in stressed materials.

Some practical implications of the anisotropy of irradiation creep were recently discussed [5,33]. In polycrystalline materials, the grain to grain variations of the creep properties lead to a local state of stress which differs both in magnitude and orientation from grain to grain. Upon removal of the external loads, internal residual stresses arise. It has been shown [33] that these residual stresses give rise to an anelastic transient creep strain in a polycrystal when the external stress is changed. This example demonstrates that the macroscopic creep behavior is not only a consequence of the atomistic process of deformation, but is also dependent on the heterogeneous nature of structural materials.

5. Conclusions

In comparing theory and experimental data of irradiation creep we have restricted ourselves to type 316 stainless steel irradiated in the fast neutron flux of EBR-II. This restriction is deemed necessary because of several reasons. First, high fluence data are presently available only from irradiation in fast reactors. Second, there appear to be different mechanisms leading to irradiation creep, namely dislocation glide and climb by SIPA. The latter makes a substantial contribution only at intermediate and high fluences. Irradiation creep data obtained in ion-bombardment experiments are presently restricted to very low doses, and therefore, the dominant creep mechanism in these experiments appears to be a glide process. Third, a comprehensive electron microscopy study of the microstructure of highly irradiated materials in both the stressed and unstressed conditions has only been done for type 316 stainless steels.

For these reasons, our conclusions may not apply to other materials, such as Zircaloy and refractory metals. Nevertheless, the understanding gained for SS 316 will certainly influence future investigations on irradiation creep in these other materials.

The above comparison of theory and experimental evidence for various mechanisms of irradiation creep leads us to the following conclusions:

1) The interstitial-type loops represent only a partial record of the more recent stress history. Hence, the microstructure observed at a given dose can only provide information about the irradiation creep rate at this dose, but not about the accumulated creep strain.

2) Both glide and climb contribute to the irradiation creep strain. However, at low doses, the climb contribution is small, though essential as a rate-controlling mechanism.
3) At intermediate and high doses, the climb contribution is substantial. This was demonstrated by a careful evaluation of the SIPA mechanism. In addition, the climb distance required for an edge dislocation to overcome the dominant glide obstacle, a Frank loop, is of the same order as the glide distance between two subsequent glide obstacles. Hence, climb and glide must contribute to the irradiation creep strains.
4) Whereas the SIPA mechanism yields a linear stress dependence in an unequivocal manner, the same cannot be said for any of the glide mechanisms.
5) Both the theoretical basis as well as the experimental evidence of stress-induced loop alignment are in favor of the SIPA mechanism rather than a loop rotation mechanism.
6) Climb-controlled glide and climb-induced yielding are opposite extremes of the same mechanism for irradiation creep. For the former, the climb process at one dislocation only induces its own glide motion, whereas in the latter case, it triggers the glide motion of other dislocations as well. Which view is the more appropriate one depends on the extent of the heterogeneous nature of the microstructure.
7) Because of the crystallographic dependence of the irradiation creep properties, a polycrystalline material is indeed heterogeneous. The extent of the variation of irradiation creep from grain to grain depends on the atomistic mechanism for irradiation creep. The macroscopic irradiation creep law of a polycrystal then contains

terms which lead to anelastic behavior as a result of this heterogeneity.

8) The dose and temperature dependence of irradiation creep is mainly determined by the evolution of the loop and dislocation structure, and at very high doses, also by the radiation-induced phase changes.

Acknowledgements

This work was supported by the Division of Basic Energy Sciences, Department of Energy, under contract ER-78-S-02-4861. The author has greatly benefited from discussions with many researchers, in particular with H.R. Brager, F.A. Garner, and E.R. Gilbert from the Hanford Engineering and Development Laboratory, and with L.K. Mansur and T.C. Reiley from the Oak Ridge National Laboratory.

References

[1] E.E. Bloom and W.G. Wolfer, Report ORNL/TM-6296, June (1978).

[2] H.R. Brager and J.L. Straalsund, J. Nucl. Mater. 46 (1973), 134.

[3] H.R. Brager, E.R. Gilbert, and J.S. Straalsund, Rad. Effects 21 (1974), 37.

[4] H.R. Brager, F.A. Garner, and G.L. Gutherie, J. Nucl. Mater. 66 (1977), 301.

[5] W.G. Wolfer and G.A. Garner, J. Nucl. Mater., to be published.

[6] J.H. Gittus, Phil. Mag. 28 (1973), 261.

[7] A.C. Roberts and A.H. Cottrell, Phil. Mag. 1 (1956), 711.

[8] R.V. Hesketh, Rep. BNL50083 (1967), 389.

[9] V. Quéré and J. Pouseye, Rad. Effects 1 (1969), 141; J. Pouseye, Rad. Effects 8 (1971), 13.

[10] W.G. Wolfer, J.P. Foster, and F.A. Garner, Nucl. Techn. 16 (1972), 55.

[11] A.D. Brailsford and R. Bullough, Phil. Mag. 27 (1973).

[12] W.G. Wolfer and A. Boltax, Europ. Conf. on Irrad. Embrittlement and Creep in Fuel Cladding and Core Components, London, 1972, Paper 31.

[13] P.R. Okamoto and S.D. Harkness, J. Nucl. Mater. 48 (1973), 204.

[14] W.G. Wolfer, L.K. Mansur, and J.A. Sprague, Intern. Conf.: Rad. Effect in Breeder Reactor Structural Materials, ed. by M.L. Bleiberg and J.W. Bennet, AIME, 1977, p. 841.

[15] F.A. Garner, W.G. Wolfer, and H.R. Brager, Report HEDL-SA-1414, Proc. of the ASTM 9th Intern. Symp. on Effects of Radiation on Structural Matls., Richland, (1978).

[16] R.A. Johnson, Phys. Rev. 152 (1966), 629.

[17] K-H. Robrock, L.E. Rehn, V. Spiric, and W. Schilling, Phys. Rev.B15 (1977), 681.

[18] P.T. Heald and M.V. Speight, Phil. Mag. 29 (1974), 1075.

[19] W.G. Wolfer and M. Ashkin, J. Appl. Phys. 46 (1975), 446.

[20] W.G. Wolfer and M. Ashkin, J. Appl. Phys. 47 (1976), 791.

[21] R. Bullough and J.R. Willis, Phil. Mag. 31 (1975), 855.

[22] P.T. Heald and M.V. Speight, Acta Met. 23 (1975), 1389.

[23] W.G. Wolfer, Scripta Met. 9 (1975), 801.

[24] J.L. Straalsund, Intern. Conf.: Rad. Effects in Breeder Reactor Structural Materials, ed. by M.L. Bleiberg and J.W. Bennet, AIME 1977, p. 191.

[25] E.R. Gilbert and A.J. Lovell; Intern. Conf.: Rad. Effects in Breeder Reactor Structural Materials, ed. by M.L. Bleiberg and J.W. Bennet, AIME 1977, p. 269.

[26] J.H. Gittus, Phil. Mag. 25 (1972), 345.

[27] L.K. Mansur, Report ORNL/TM-6443, August 1978.

[28] W.G. Wolfer, M. Ashkin, and A. Boltax, in Properties of Reactor Structural Alloys After Neutron or Particle Irradiation, ASTM STP 570 (1976), 233.

[29] J. Weertman, in Rate Processes in Plastic Deformation of Materials, ed., by J.C.M. Li and A.K. Mukherjee, ASTM 1975, p. 315.

[30] H.R. Brager, F.A. Garner, E.R. Gilbert, J.E. Flinn, and W.G. Wolfer, Radiation Effects in Breeder Reactor Structural Materials, ed. by M.L. Bleiberg and J.W. Bennett, AIME 1977, p. 727.

[31] W.A. Coghlan and M.H. Yoo, Trans. ANS 27 (1977), 330.

[32] A. Seeger and U. Goesele, Phys. Letters 61A (1977), 423.

[33] W.G. Wolfer, Report UWFDM-254, Proc. of the ASTM 9th Intern. Symp. on Effects of Radiation on Structural Matls., Richland 1978.

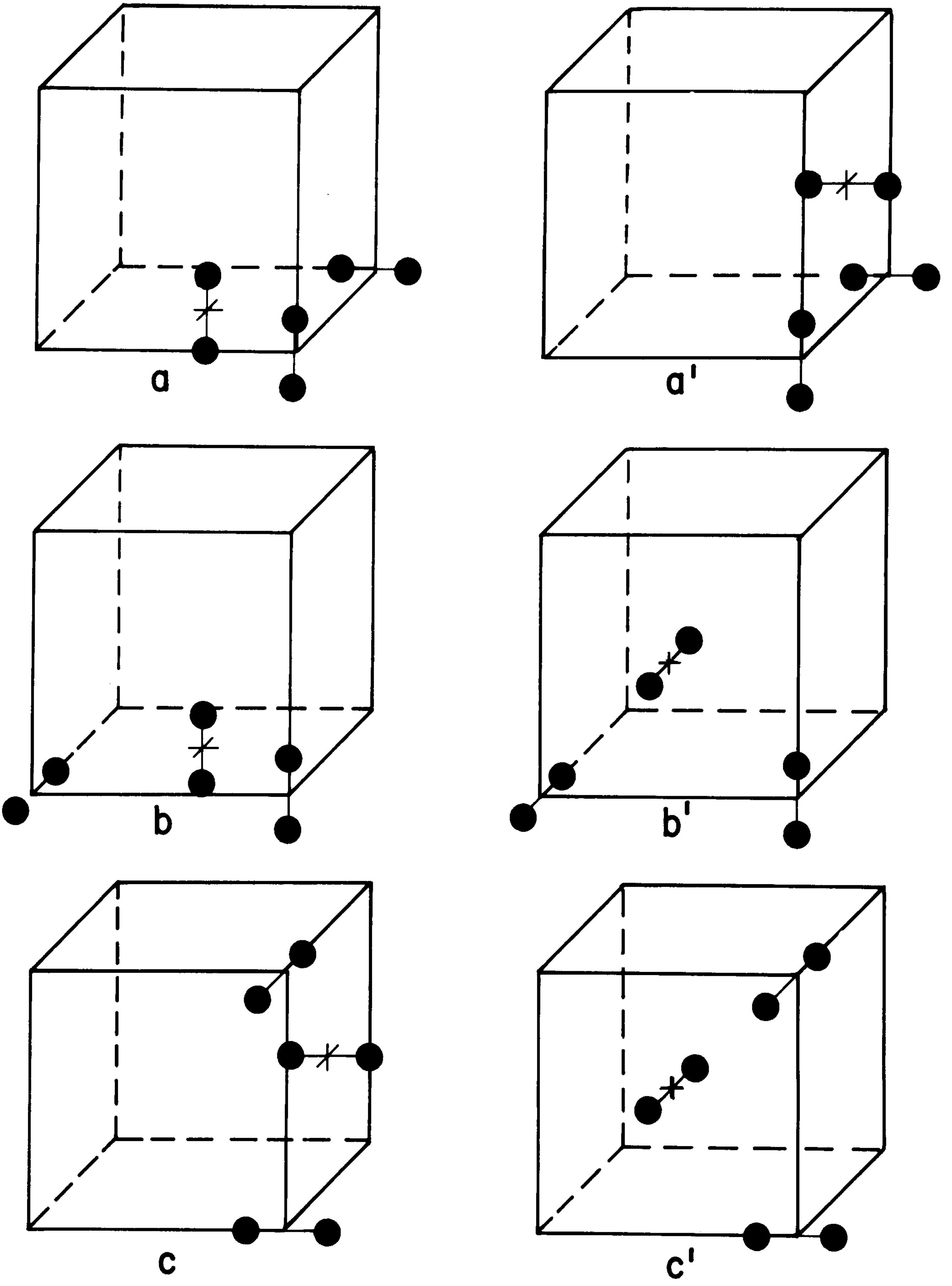

Fig. 1. The six stable tri-interstitial configurations in fcc metals.

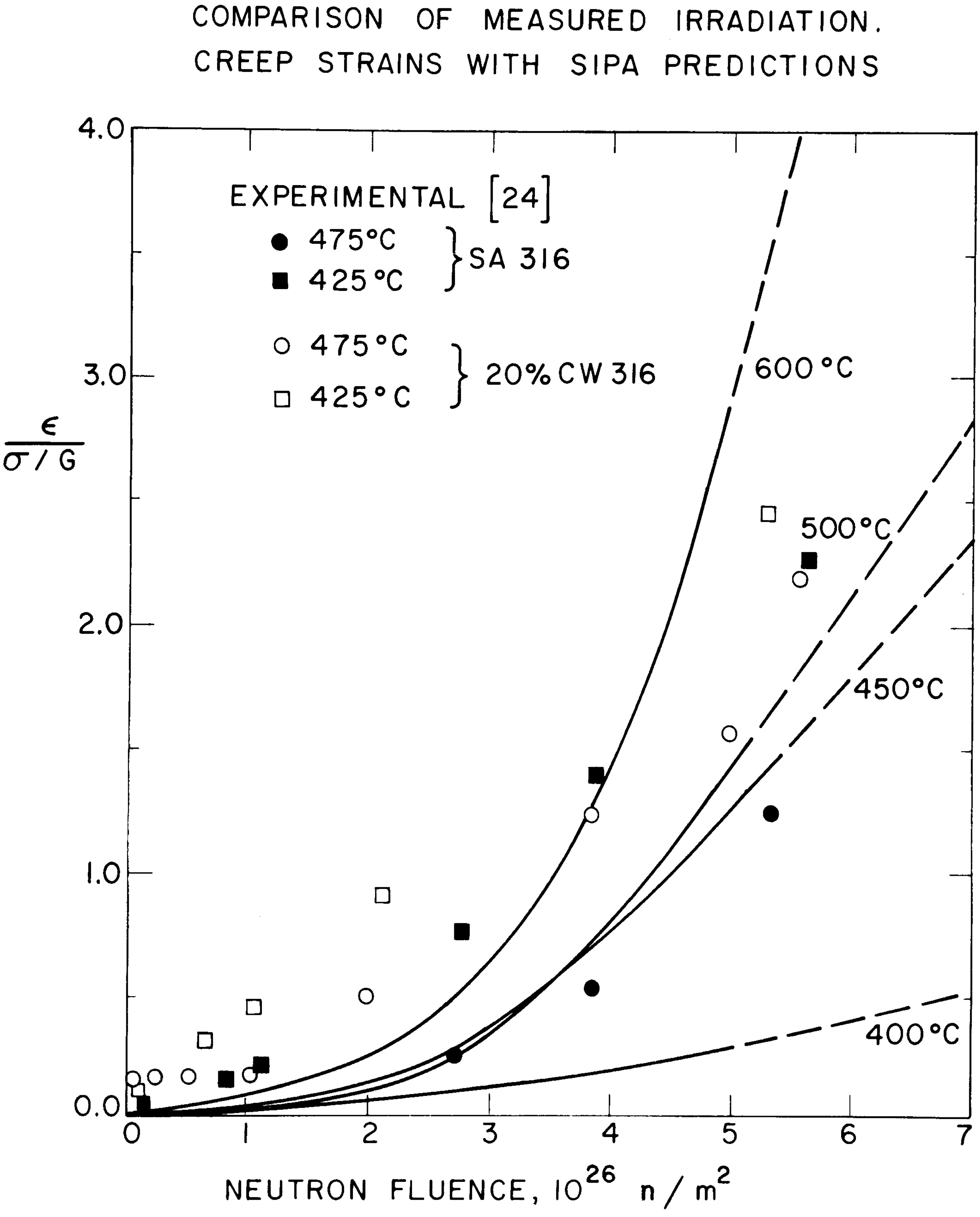

Fig. 2. Comparison of the predicted and the measured irradiation creep strain as a function of fluence. The solid lines are due to SIPA creep, using the microstructural data of Ref. 2.

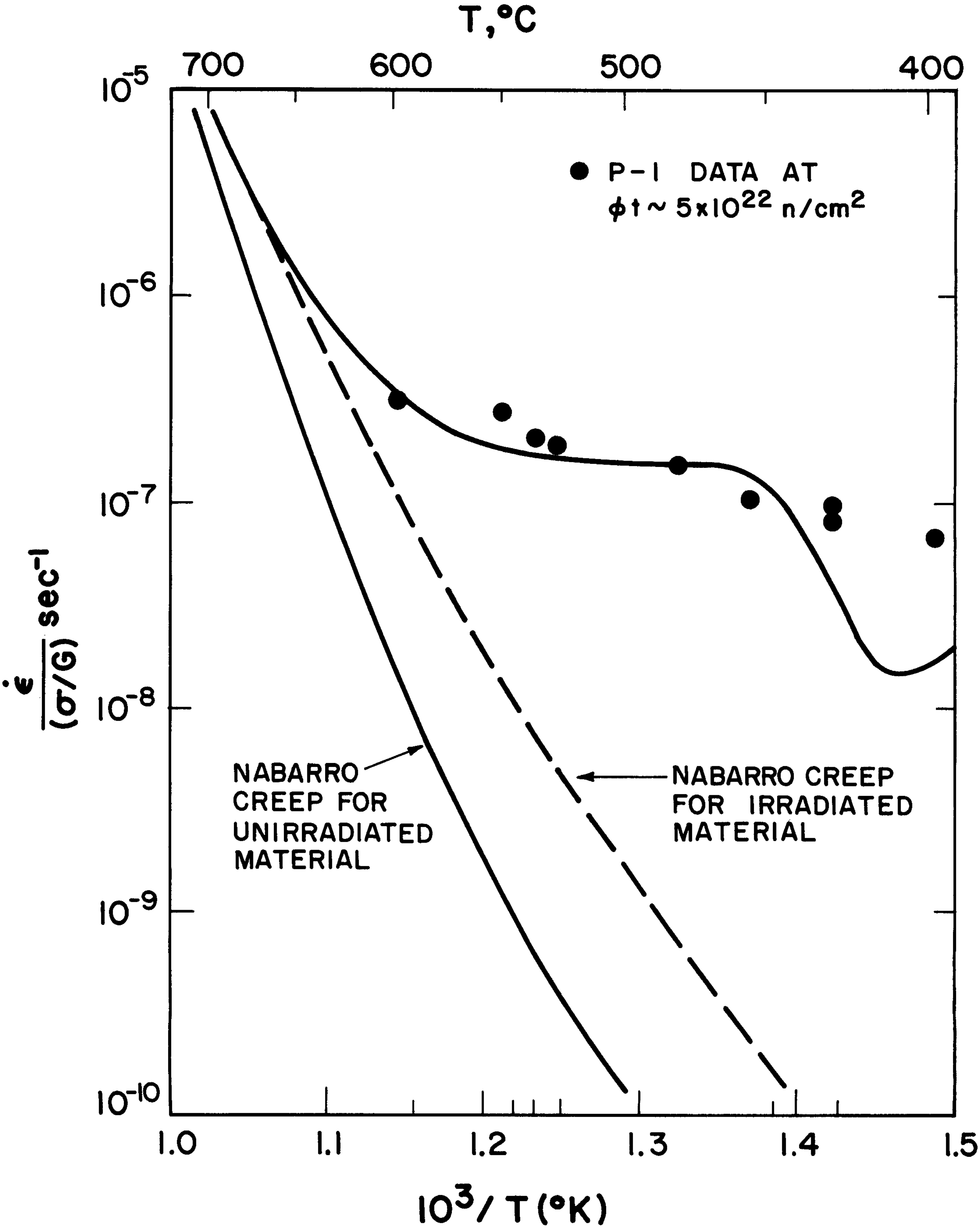

Fig. 3. Comparison of the temperature dependence of predicted SIPA creep and the measured irradiation creep strain rates.

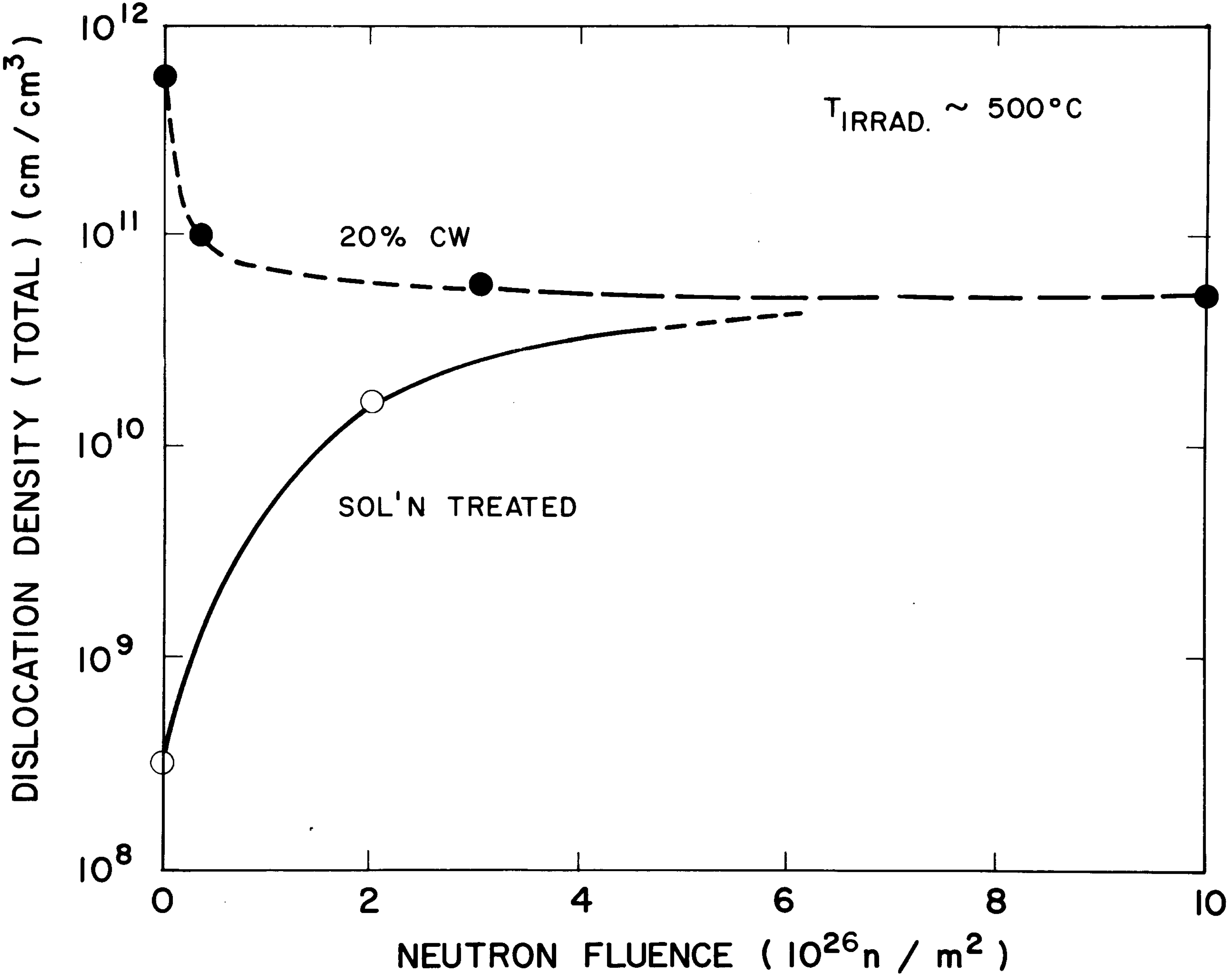

Fig. 4. The evolution of the measured dislocation density for solution annealed and 20% CW stainless steel [30] as a function of fluence for an irradiation temperature of 500°C.

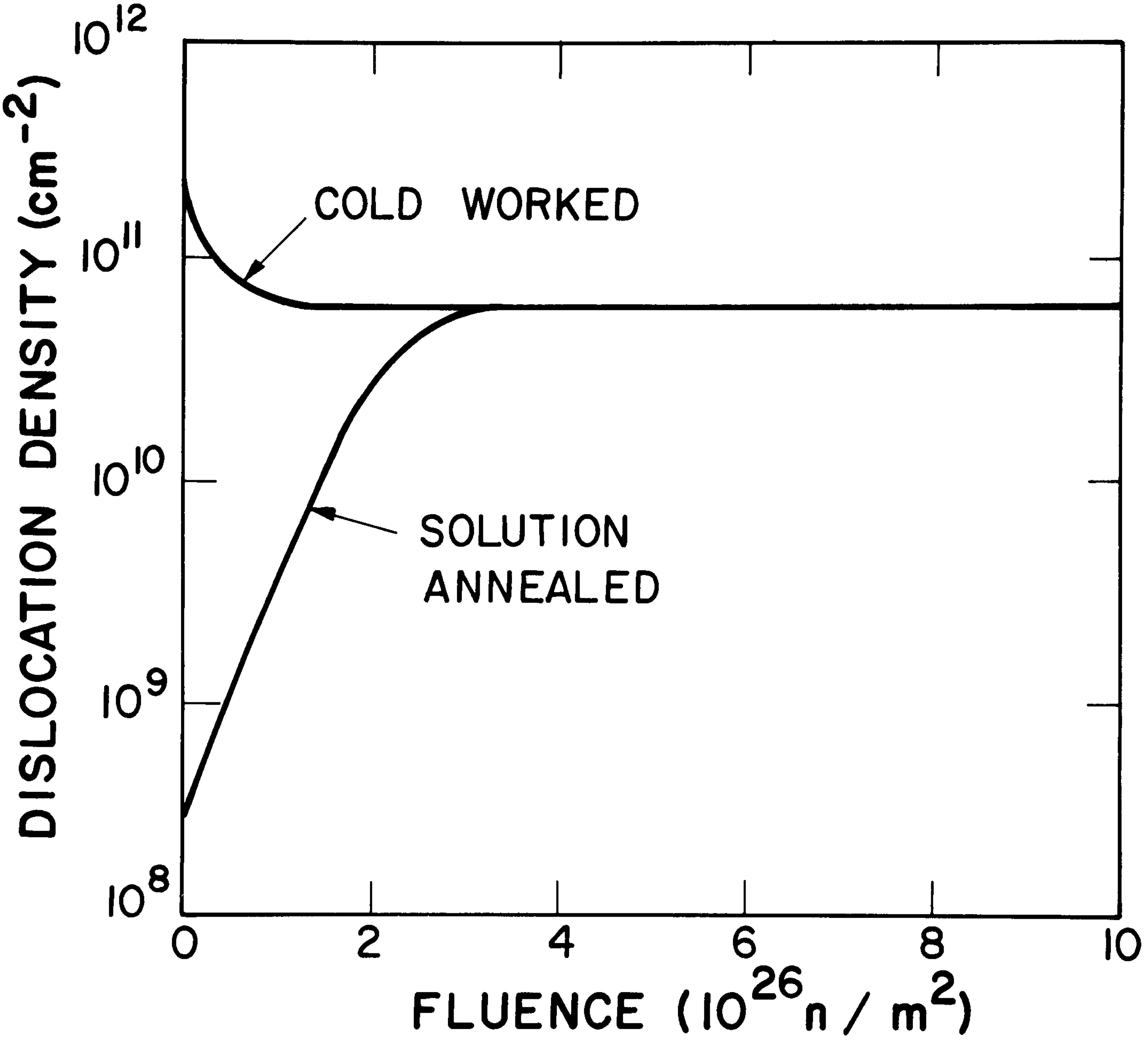

Fig. 5. The evolution of the dislocation density as computed from theory.

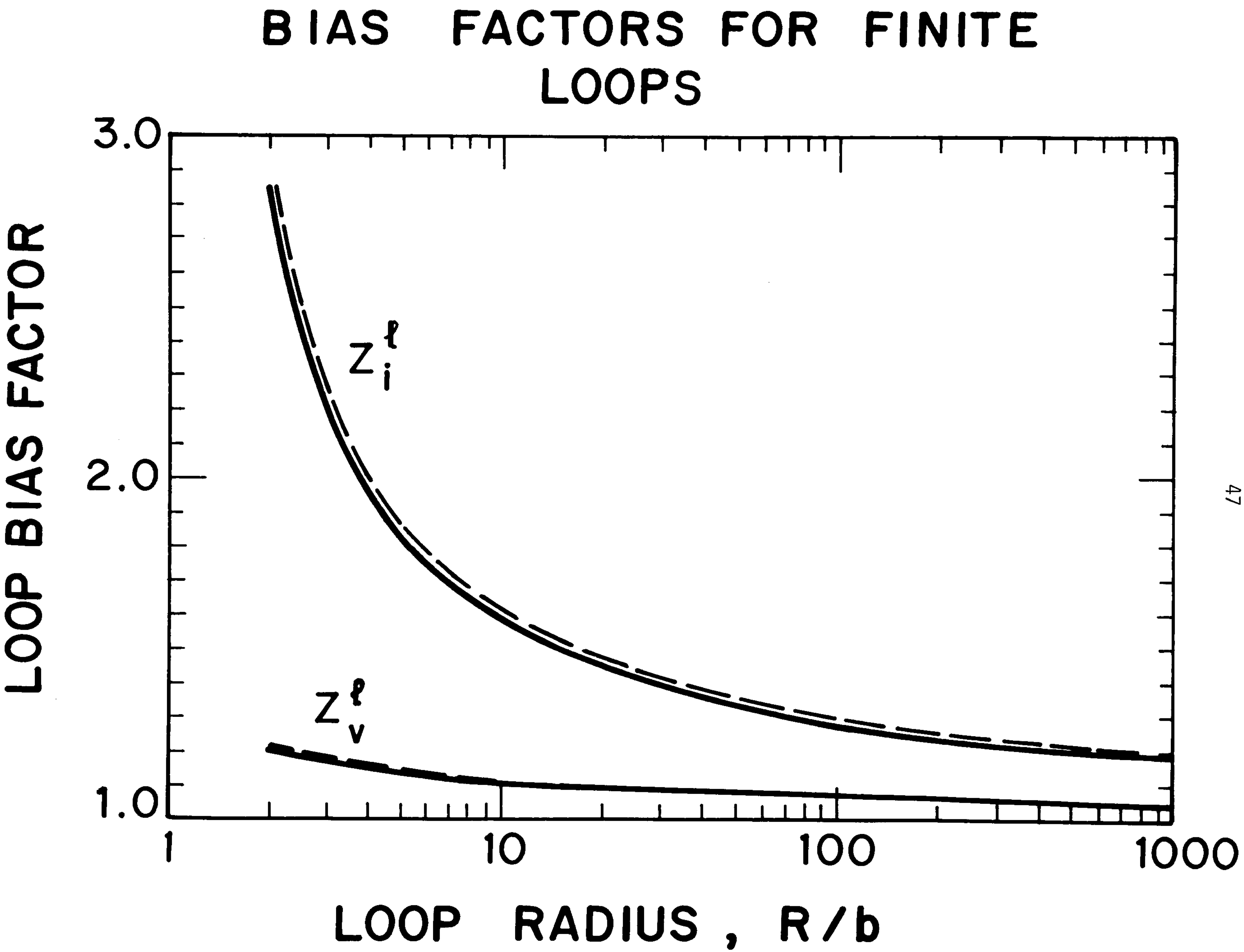

Fig. 6. The bias factors of a dislocation loop for interstitials, Z_I^ℓ, and for vacancies, Z_V^ℓ, as a function of the loop size.

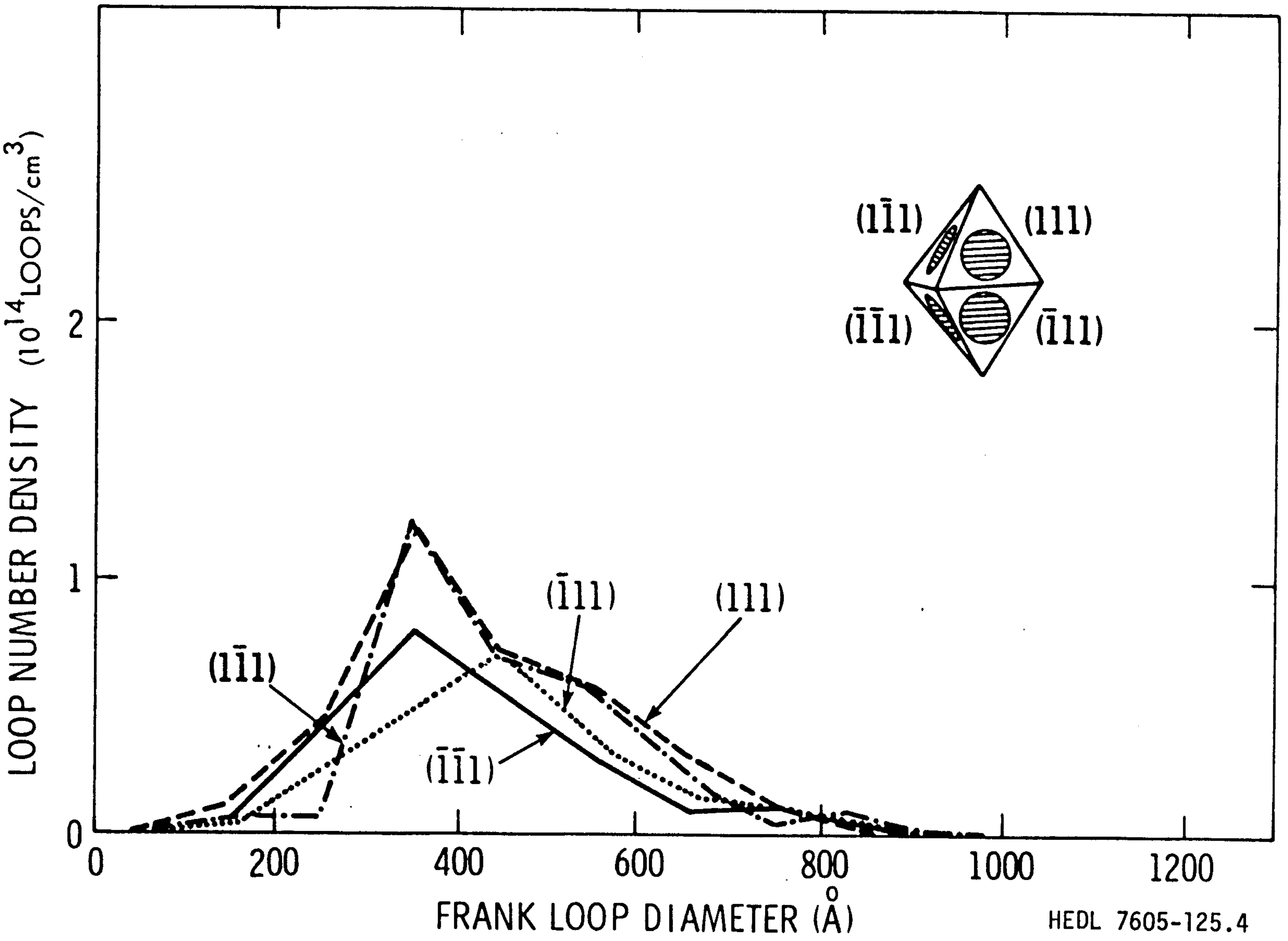

Fig. 7. Frank loop distributions in unstressed 20% CW 316 stainless steel irradiated at 500°C to 3 x 10^{26} n/m^2. Courtesy of Brager et al. [4].

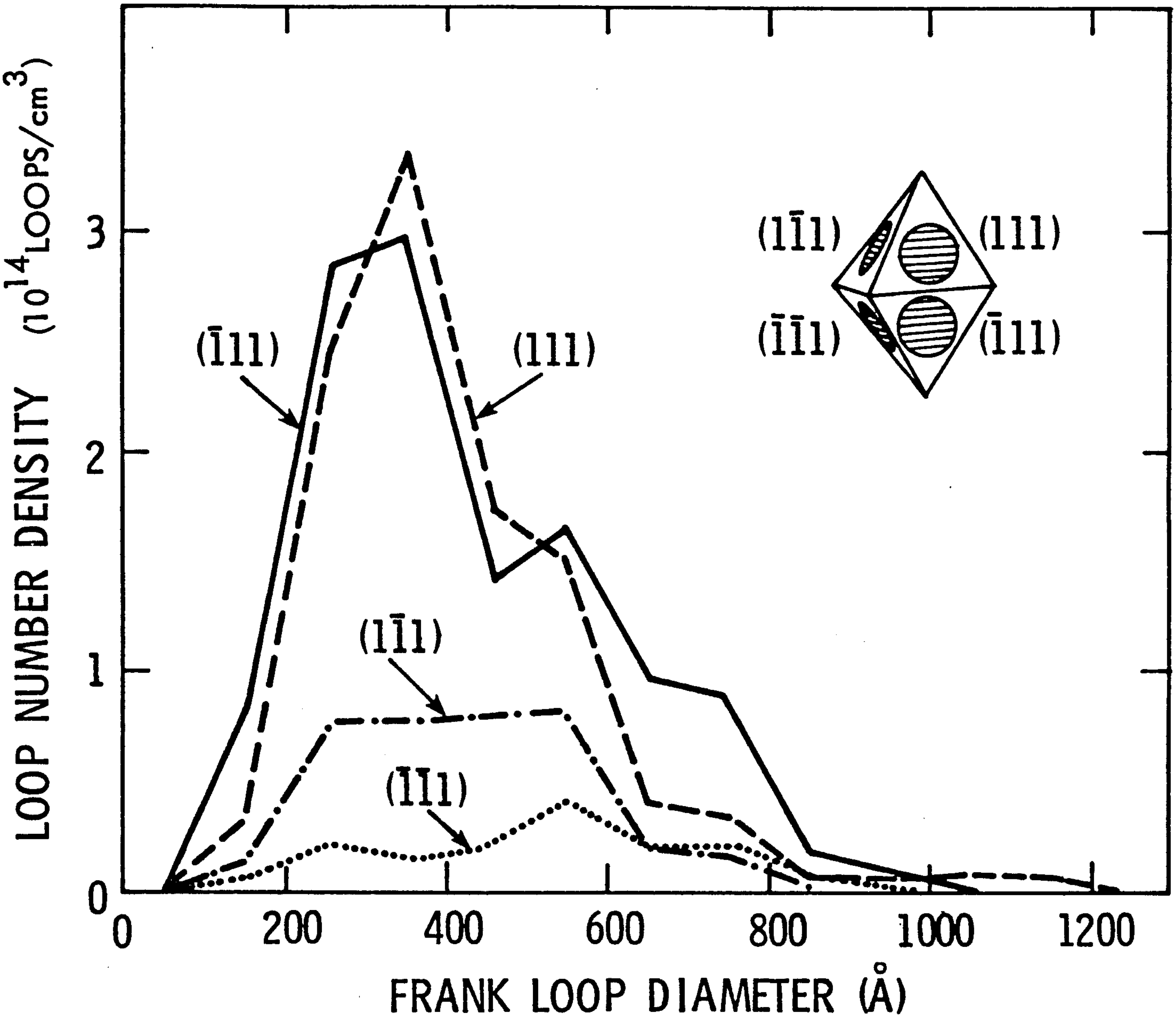

HEDL 7605-125.6

Fig. 8. Frank loop distributions in stressed 20% CW 316 stainless steel irradiated at 500°C to 3 x 10^{26} n/m^2 and under a hoop stress of 327 MN/m^2. Courtesy of Brager et al. [4].

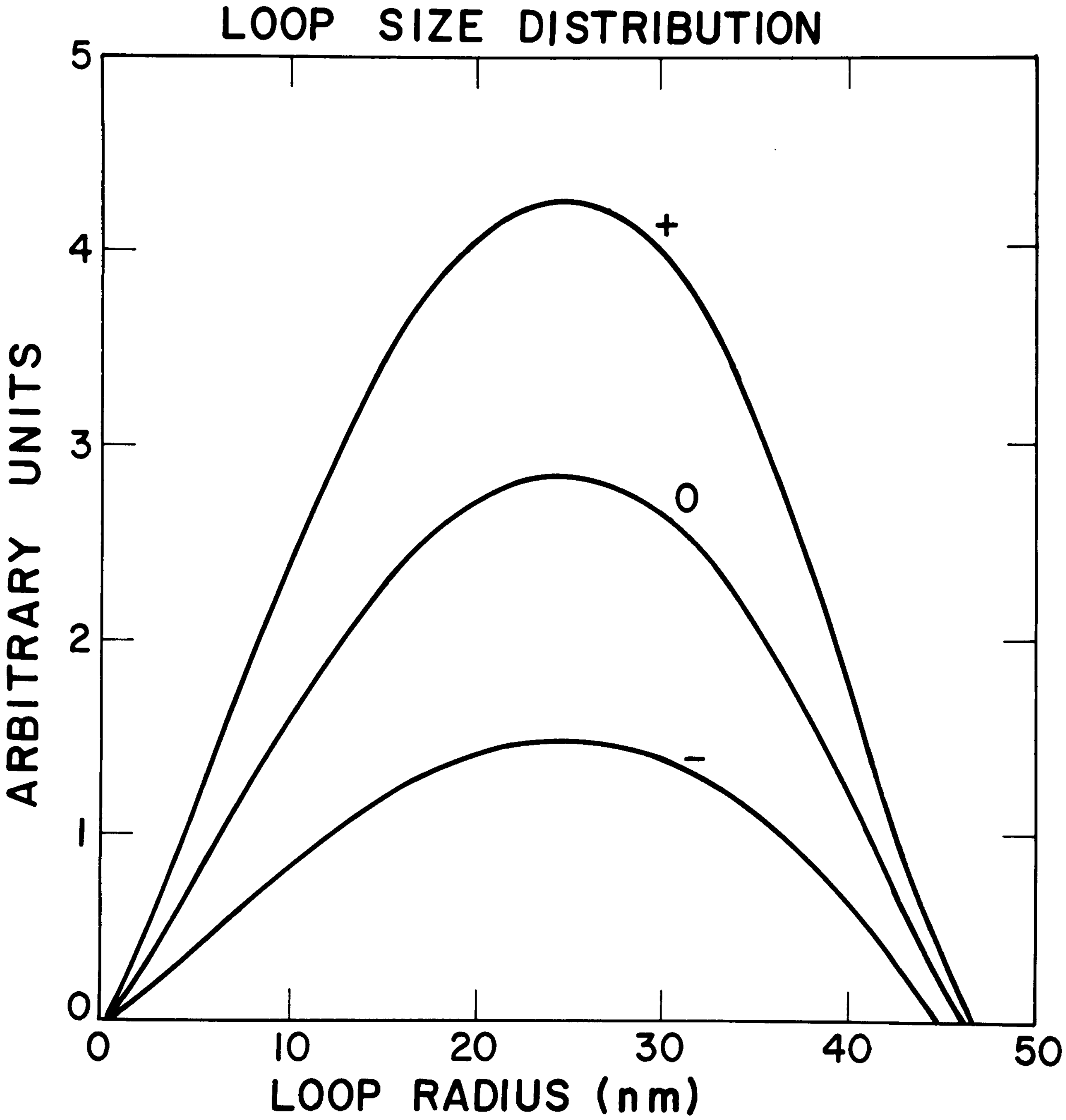

Fig. 9. Computed loop size distributions for normal stresses equal to zero (0), $\sigma_n/G = 0.001$ (+), and $\sigma_n/G = -0.001$ (-).